2019 IEEE/RSJ International Conference on Intelligent Robots and Systems (IROS)
Macau, China, November 4-8, 2019

Motion Planning for a Continuum Robotic Mobile Lamp: Defining and Navigating the Configuration Space

Zachary Hawks[† 1], Chase Frazelle[2], Keith E. Green[3] and Ian D. Walker[4]

***Abstract*— We discuss motion planning in the configuration spaces of robots containing continuum elements. The configuration space structure of extensible continuum sections is first analyzed, with practical constraints unique to continuum elements identified. The results are applied to generate the configuration space of a hybrid continuum lamp/mobile base robot. A conventional motion planning RRT/A* approach is subsequently applied for the robot in an aging in place application scenario.**

I. INTRODUCTION

This paper addresses the nature of the configuration space of, and its use in motion planning for, continuum robots. Continuum robots are composed of one or more continuum sections. A continuum section is kinematically described by continuous and smooth curvature [1], [2]. Continuum robots theoretically possess infinite degrees of freedom (DoF), unlike standard rigid-link robots which have finite DoF. Continuum sections are most often tendon or pneumatically driven, or composed of concentric tubes. These robots are often inspired by elements in biology, like plant tendrils, an elephant trunk, or octopus tentacles. Because of their underlying curvature, continuum robots are often compliant in nature and are used to explore hard-to-reach areas [3], [4].

For conventional, non-continuum robots, classical motion planning techniques using configuration space have been well studied [5]. For example, rapidly exploring random tree (RRT) algorithms have been shown to successfully span the configuration space for mobile robots and rigid-link robots [6]. The A* algorithm, given a graph and proper heuristic function, will guarantee the optimal path between any 2 nodes if one exists [6].

In the past, a variety of motion planning techniques have been implemented for continuum robots. The motion planning problem for active cannulas (concentric tube robots in medical applications) within tubular environments is formulated as an constrained optimization problem in [7]. Constrained optimization is also used in [8] to formulate and solve the motion planning problem for a soft planar continuum manipulator. Grasp planning for continuum robots using a bounding circle technique was investigated in [9] and [10]. A follow the leader approach for tendon-driven continuum robots is introduced in [11]. Researchers have used sampling based approaches based on the techniques of Rapidly-Exploring Roadmaps (RRM) [12], Rapidly-Exploring Random Graphs (RRG) [13], [14], and Rapidly-Exploring Random Trees (RRT) [15] to plan

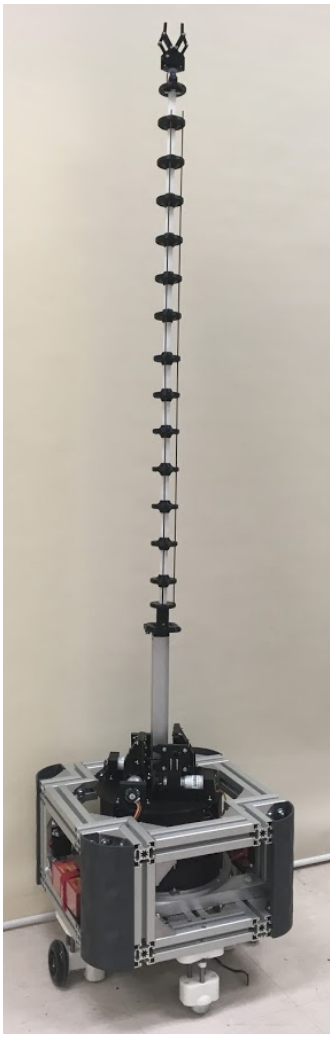

Fig. 1: **C**ontin**u**um **R**obotic **L**amp **E**lement.

This research is supported in part by the U.S. National Science Foundation under awards IIS-1703267, IIS-1527165 and IIS-1718075, and in part by NASA under contract NNX12AM01G, and in part by a NASA Space Technology Research Fellowship, contract 80NSSC17K0173

† To whom all correspondence should be addressed

[1]Zachary Hawks is with the Department of Electrical and Computer Engineering, Clemson University, Clemson, SC, 29634, USA zhawks@clemson.edu

[2]Chase Frazelle is with the Department of Electrical and Computer Engineering, Clemson University, Clemson, SC, 29634, USA cfrazel@clemson.edu

[3]Keith E. Green is with the Sibley School of Mechanical and Aerospace Engineering, Cornell University, Ithaca, NY, 14853, USA keg95@cornell.edu

[4]Ian D. Walker is with the Department of Electrical and Computer Engineering, Clemson University, Clemson, SC, 29634, USA iwalker@clemson.edu

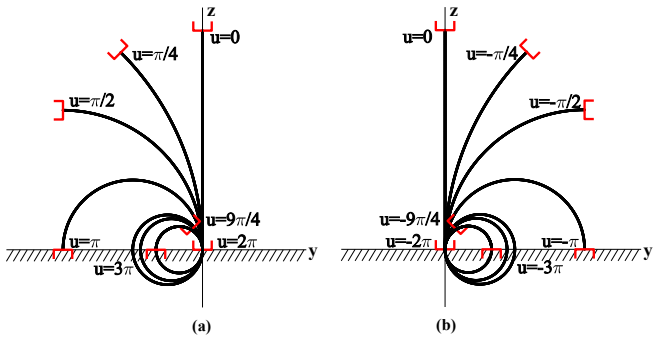

Fig. 2: Single section continuum robot bending (a) counter-clockwise and (b) clockwise in the yz-plane.

motions for concentric tube continuum robots in tubular environments for medical applications.

However, it appears that the principles of the classical motion planning techniques such as RRT and A* have not yet been applied to tendon-actuated continuum robots in general non-tubular environments. This is in part due to a lack of formal analysis of the nature of the configuration space of tendon-actuated continuum robot elements. In this paper, we define and discuss the configuration space of single section extensible continuum robots and use the configuration space to path plan using RRT. The analysis is applied to the specific example of CuRLE shown in Fig. 1. CuRLE is an element of *home+*, our collection of robotic home furnishing elements designed to assist in the home with aging-in-place [16]. In the process, we illustrate and highlight several structural constraints imposed by tendon-actuated continuum geometry. This is described further in IV after we investigate the configuration space of continuum robots in II and compare to the configuration of a kinematically similar rigid link robot in III.

II. CONTINUUM CONFIGURATION SPACE

We begin by considering the underlying structure of continuum robot configuration space in the presence of physical and actuation constraints. Specifically, we consider the c-space of the basic element of continuum robots: a single extensible section. We assume the section to be of constant curvature.

A. Single Section Continuum Robot

A single section extensible continuum robot can be described by 3 kinematic variables: $\{u,v,s\}$ where is s is the arc-length of the section and u and v represent the components of a rotation axis with respect to the base of the section [17]. Let $c \in C^3_{space}$ be a configuration in the configuration space of the robot where $c = [u\ v\ s]^T$.

To better envision C^3_{space}, let us first consider the configuration space C^1_{space} where only u varies. We restrict the length $s = s_{fixed}$ and set $v = 0$. A configuration is then defined as $c = [u] \in C^1_{space}$. As we vary u in the positive direction (equating to counter-clockwise rotation), the section will bend to the left in the yz-plane, as shown in Fig. 2a.

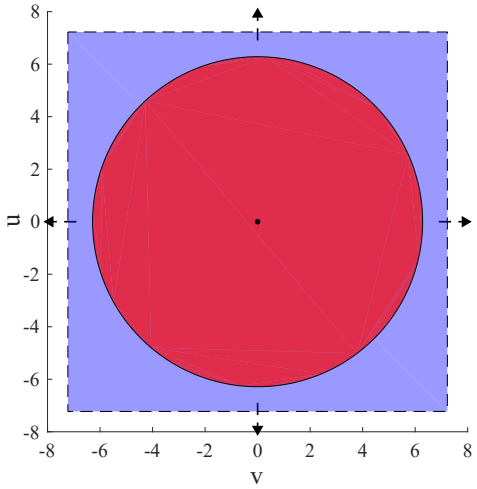

Fig. 3: A visualization of C^2_{space}. The blue plane extends to $\pm\infty$. The red circle indicates C^2_{space} with the physical constraint of $\theta \leq 2\pi$.

Once $u = 2\pi$, the section's tip will meet the base and form a perfect circle. Continuing to increase u will cause the robot to "bend within itself"' and theoretically it would continue to "encircle" itself as $u \to \infty$. Increasing u in the negative direction (clockwise) will cause the same planar motion mirrored across the z-axis (Fig 2b). As $u \to (-\infty)$, the robot will continue to encircle itself to generate the remaining set of possible planar configurations of the section. Therefore, the configuration space of the robot where only u varies is $C^1_{space} \equiv \mathbb{R}$.

If we remove the restriction on v and allow it to also vary, then the configuration space changes to a 2D space where any configuration is defined as $c = [u\ v]^T \in C^2_{space}$. The total "bend" of the robot, θ, in the plane of curvature is defined by [17].

$$\theta = \sqrt{u^2 + v^2} \tag{1}$$

When $\theta = 2\pi$, the section once more forms a perfect circle, with its tip touching the base. Varying the vector $[u\ v]^T$ generates all bending directions (planes of curvature) and increasing the magnitude of the vector generates all possible configurations in each of these planes via (1). Since $u, v \in \mathbb{R}$, $C^2_{space} \equiv \mathbb{R}^2$ and can be visualized as the infinite plane described in Fig. 3.

If we now allow s to vary as well, a configuration is defined as $c = [u\ \ v\ \ s]^T \in C^3_{space}$. Since $s \in (0,\infty)$, then $C^3_{space} \in \mathbb{R}^3$ s.t. $s > 0$.

B. Physical Constraints in a Single Section Continuum Robot

At this point, however, we must discuss constraints in the configuration space imposed by physical limitations of the robot. The first constraint to consider is on length. Any physical robot will have a maximum and minimum length, imposing an upper and lower bound on arc-length: $s_{min} \leq s \leq s_{max}$.

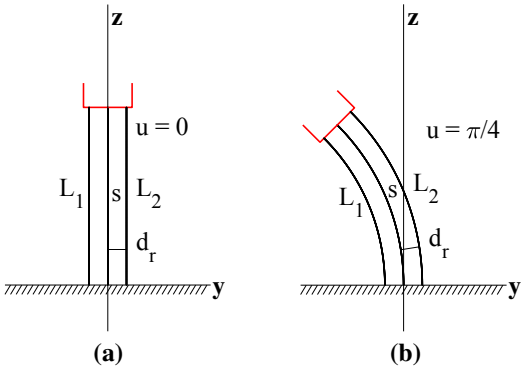

Fig. 4: An illustration of physical constraints of bending a continuum robot. In (a), $L_1 = L_2 = s$. In (b), the robot has bent counter-clockwise, causing L_2 to lengthen and L_1 to shorten, while s remains constant.

Another constraint is imposed by the physical width of the backbone of tendon actuated continuum robots. This physical distance, $d_r > 0$, is the distance from the center of the backbone to its outer edge. With s being the length down the exact center of the backbone, and L_1 and L_2 the tendon lengths along its outside in the plane of bending (Fig. 4), when the robot is perfectly straight (i.e. $u = v = 0$), then $L_1 = L_2 = s$. For the robot to bend counter-clockwise in the plane, the length of the left side of the robot, L_1, must shorten at the same rate that the length of the opposite side of the robot, L_2, lengthens. This is illustrated in Fig. 4.

Because of this, the section cannot bend at all when it is at maximum or minimum length. When $s = s_{max}$ and $u = v = 0$, then $L_1 = L_2 = s_{max}$. To bend, L_1 or L_2 must lengthen, but each is already at the maximum length. The same reasoning is applied when $s = s_{min}$. At maximum/minimum length, $C^3_{space} = \{ \begin{bmatrix} 0 & 0 & s_{max/min} \end{bmatrix}^T \}$. The practical configuration space can now be visualized in Fig. 5(a). When $s = \frac{s_{max} - s_{min}}{2}$ the robot will be able to achieve the greatest amount of bending and will have the largest "uv-plane."

A further practical constraint arises due to "encircling" imposed when $\theta > 2\pi$. Depending on the specific physical construction of a practical continuum section, it is likely that it will not be able to "encircle" itself. Even if it could, it cannot continue doing so as $u, v \to (\pm)\infty$. Therefore, there will exist some boundary for u and v imposed by physical constraints. For our purposes, we set this boundary to be at $\theta = 2\pi$, which bounds C^2_{space} as shown in Fig. 3. Expanding the $\theta \leq 2\pi$ constraint to C^3_{space} gives the space seen in Fig. 5(b), which is the practical configuration space for a single section extensible continuum robot with physical constraints exploited herein.

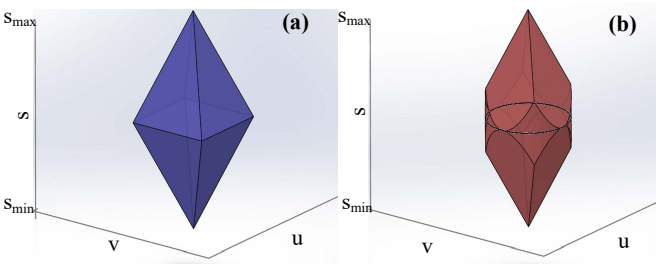

Fig. 5: A visualization of C^3_{space}. In (a) the physical constraints of the backbone are illustrated. The maximum bend can be achieved when $s = \frac{s_{max} - s_{min}}{2}$, which is the widest plane in the center of the pyramid. In (b), the physical constraint of $\theta \leq 2\pi$ is applied to (a), which forms the "rounded" pyramid shape. The largest "uv-plane" indicated circle in (b) is the same circle shown in Fig. 3.

III. A COMPARISON: EQUIVALENT RIGID LINK ROBOT CONFIGURATION SPACE

To highlight the unique issues presented by continuum section structures, we compare with the case of a kinematically similar rigid link robot.

A. Equivalent Rigid Link Robot

To analyze a rigid link robot structure with the same DoF as the continuum robot section, we use for comparison a 3 DoF robot with a constrained RRPRR joint configuration, where R and P indicate revolute and prismatic joints, respectively. This kinematic arrangement extends to 3D the modeling of a planar extensible continuum section by planar RPR kinematics described in [18]. The underlying concept is for the prismatic joint to provide the translation between the ends of the section, and the initial and final pairs of revolute joints to rotate the prismatic joint in the appropriate direction (θ_1) and align the initial and final tangents of the section (θ_2) [18]. To achieve this, we constrain the third and fourth revolute joints to exactly match the values of the first and second revolute joints, respectively, which gives the configuration vector $q = [\theta_1 \;\; \theta_2 \;\; d \;\; \theta_1 \;\; \theta_2]^T$. The prismatic joint can extend/retract between a maximum and minimum length. We select this rigid link configuration since we can construct a kinematic mapping between its configuration space and the configuration space of the continuum robot section that restricts the rigid link robot to the equivalent task space of the continuum section. This mapping, F, is described in section III-D. Fig. 6 shows the two robots sharing the same task space for different values of u. Note that in each case the end effector positions and orientations are identical, and shown in red.

B. Configuration Space

For the two independent revolute DoF: $\theta_1, \theta_2 \in [0, 2\pi)$ and $q = [\theta_1 \;\; \theta_2]^T \in Q^2_{space}$. Rather than the infinite plane in Fig. 3, the space manifests as a square with "wrapping" phenomenon that causes $\theta_1, \theta_2 \geq 2\pi, \vee\, \theta_1, \theta_2 < 0$ to "wrap"

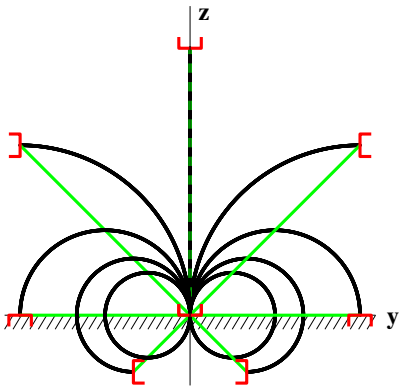

Fig. 6: The task space of both the continuum section (black) and rigid link structure (green) for different values of u.

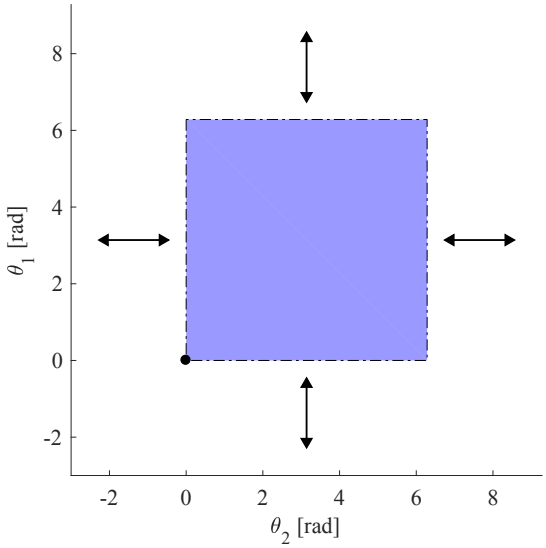

Fig. 7: Q^2_{space} of the rigid-link robot.The arrows indicate the "wrapping" phenomenon that occurs when θ_1 and θ_2 go beyond the bounds $[0, 2\pi)$.

back to $0 \leq \theta_1, \theta_2 < 2\pi$, as seen in Fig.7. This space, while 2D, is best visualized as the surface of a torus,

Adding the prismatic joint modifies the square in Fig. 7 into the rectangular prism shown in Fig. 8. As with the Q^2_{space}, the same "wrapping" phenomenon occurs whenever one of the joints goes beyond 0 or 2π. The configuration space can be defined as $\forall q = [\theta_1 \;\; \theta_2 \;\; d]^T \in Q^3_{space}$ s.t. $0 \leq \theta_1 < 2\pi,\;\; 0 \leq \theta_2 < 2\pi,\;\; d_{min} \leq d \leq d_{max}$.

C. C-Space of Continuum Section vs Rigid-Link Structure

The key difference between the continuum and rigid-link configuration spaces (c-space) is the "wrapping" phenomenon that occurs in Q^3_{space}. In the ideal continuum c-space, there exists exactly one straight path connecting any two configurations $c_1,\, c_2 \in C^3_{space}$. For the rigid-link robot,

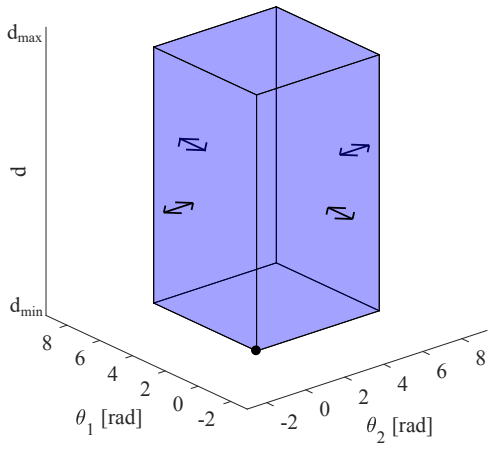

Fig. 8: Q^3_{space} of the rigid-link robot. The arrows indicate the "wrapping" phenomenon that occurs when θ_1 and θ_2 go beyond the bounds $[0, 2\pi)$.

there are always 2 straight paths between any configurations that involve a change in θ_1 or θ_2 (crossing the boundary in opposite directions in figure 7). For configuration changes that exclusively involve the prismatic joint, there is exactly 1 path.

An interesting difference between the c-spaces is their sizes. Since both C^3_{space} and Q^3_{space} are finite, their sizes can be compared by calculating the volume of each space. This can be done by calculating the volume of the 3D shapes shown in Fig. 5(b) and Fig. 8. The size of Q^3_{space} is the volume of the rectangular prism. The size of C^3_{space} is volume of the "rounded" pyramid, which is slightly less than the full 2- sided square pyramid but greater than a 2 sided cone where the base has $radius = 2\pi$.

$$(4\pi^2)(s_{max} - s_{min})\left(\frac{\pi}{3}\right) < V_{\text{cont}} < (16\pi^2)(s_{max} - s_{min})\left(\frac{1}{3}\right)$$
$$V_{\text{rigid}} = (4\pi^2)(d_{max} - d_{min}) \tag{2}$$

Since the rigid-link robot was chosen to be kinematically similar to the continuum robot, we can set the limits of the equivalent rigid link prismatic joint to those of the continuum section (they will be the same at zero curvature). We then conclude that the configuration space for a kinematically equivalent continuum section is larger than the rigid-link robot's configuration space (3). This interesting observation suggests advantages, from a configuration space planning point of view, for continuum structures over equivalent traditional rigid link ones.

$$s_{max} = d_{max} \;\;,\;\; s_{min} = d_{min}$$
$$\Rightarrow V_{\text{rigid}} < V_{\text{cont}} \tag{3}$$

D. Making Equivalent Task Space

The only difference between the two task spaces is the physical shape of the arm of the robot that creates them. This is either a constant curvature curve between the base and the end-effector (continuum) or a straight line (rigid-

link), as shown in Fig. 6. This shape is important in the context of motion planning, as it has to be accounted for when checking for collision-free paths through the space.

For the rigid-link robot to have the same task-space as the continuum robot, we construct a function F that maps every configuration $c \in C^3_{space}$ to a configuration $q \in Q^3_{space}$. This function, F, is neither one-to-one nor onto, and is shown in (4).

$$F : C^3_{space} \rightarrow Q^3_{space} \text{ s.t. } F(c) = q \text{ where}$$
$$c = \begin{bmatrix} u \\ v \\ s \end{bmatrix} \in C^3_{space} \text{ and } q = \begin{bmatrix} \theta_1 \\ \theta_2 \\ d \end{bmatrix} \in Q^3_{space}$$
$$\Rightarrow F(c) = \begin{bmatrix} \frac{u}{2} \\ \frac{v}{2} \\ \left(\frac{2s}{\sqrt{u^2+v^2}}\right) sin\left(\frac{\sqrt{u^2+v^2}}{2}\right) \end{bmatrix} \quad (4)$$

Let $Q^C_{space} \triangleq \mathbb{R}\{F\}$ where $\mathbb{R}\{F\}$ is the range of the function F. Then $Q^C_{space} \in Q^3_{space}$ is a subspace of Q^3_{space}. Since C^3_{space} is centered at $u = v = 0$, and has a radius of 2π, Q^C_{space} will be centered at $\theta_1 = \theta_2 = 0$. Now, $\theta_1, \theta_2 \in [-\pi, \pi)$. While this appears to have the same effect as $\theta_1, \theta_2 \in [0, 2\pi)$ and as such seems arbitrary to define, it is a necessity for the prismatic joint to achieve the proper configuration. From (4), we see that d directly depends on the magnitude of u and v. So while $\theta_1 = -\pi/4$ and $\theta_1 = 7\pi/4$ are the same configuration with respect to the revolute joint, they lead to unique configurations of the prismatic joint.

(1) creates another restriction found in Q^C_{space} that is absent in Q^3_{space}. Sending θ through F produces the boundary $\sqrt{\theta_1^2 + \theta_2^2} \leq \pi$. This removes the "wrapping" phenomenon and causes Q^C_{space} to have the same "rounded" pyramid shape as C^3_{space}, as shown in Fig. 9.

Finally, the volume of Q^C_{space} is significantly smaller than the volume of the C^3_{space}, but the task space is equivalent.

IV. EXPERIMENTS/VALIDATION

Our key motivation for analyzing the configuration space is to apply traditional motion planning techniques to continuum robotics in healthcare applications. Specifically, we next apply the understanding generated above to motion planning for the robot shown in Fig. 1 as a part of a wider research effort in robotic assistance for aging in place.

With the societal move towards smart devices in every home, we envision a collection of robotic furnishing elements that can provide at-home care and assistance. As we age, we lose the ability to perform simple day-to-day tasks and eventually reach a point where we can no longer live without assistive care. Our suite of robots, collectively called *home+*, collaborate with individuals over time in the home to help with these day-to-day tasks and prolong the time that the individual can live independently [16]. For instance, people need help retrieving objects from high shelves, so we created a robotic lamp, which we term CuRLE, that includes the ability to do such tasks (in addition to functioning as a lamp).

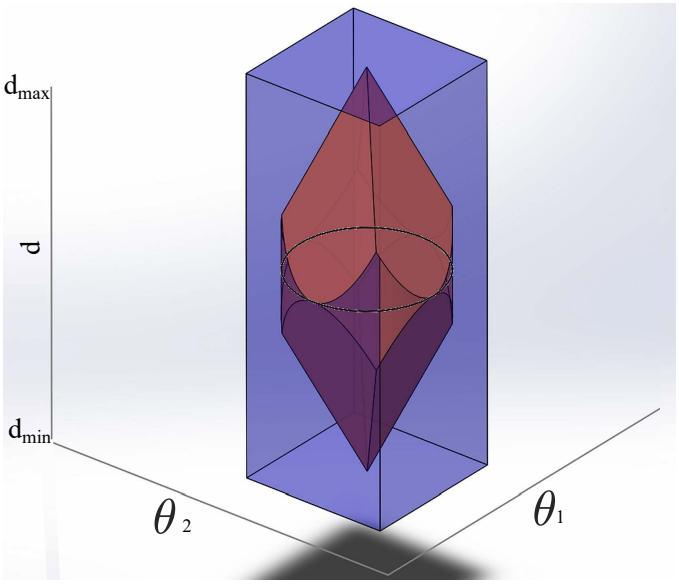

Fig. 9: The configuration space (red) of the rigid-link structure, Q^C_{space}, once it has been restricted by F to have the equivalent task space as the continuum section. This is displayed within the full c-space (blue), Q^3_{space}, from Fig. 8

A. Continuum Robotic Lamp Element (CuRLE)

CuRLE is a tendon-driven, non-extensible, single-section continuum arm mounted onto a mobile base which is controlled by a differential drive. CuRLE 's end-effector is a 2-fingered gripper featuring a series of LEDs to give the lamp light. The continuum arm is mounted on a prismatic joint (L) which serves to raise/lower the base of the continuum arm but does not change the arc length s. The prismatic joint is further mounted on a revolute joint (ω) which allows the entire arm to be rotated about the z-axis (yaw). Another revolute joint (γ) is mounted at the end of the continuum arm to serve as a "wrist" for the gripper.

1) Adding Constraints: In order to visualize the configuration space of CuRLE and conduct motion planning through the home environment space, we constrain several DoF. For the remainder of this work, we fix L to its minimum length. Since the continuum arm is non-extensible, the arc-length s is also constrained to be constant. The revolute joint γ serving as the wrist for the gripper adds redundancy, but remains fixed in the experimentation described here.

With these restrictions, we discuss the mobile base and the kinematic variables $[\omega\ u\ v]$ for the continuum arm. Since the base serves to move the continuum portion through the home space and the continuum element performs manipulation, we divide the configuration space into two parts. We assume that there will not be obstacles that CuRLE has to "pass under" meaning that nothing in the task space would collide with the continuum arm but not the mobile base. As such, we form the configuration space of the mobile base $c_b = [x\ y\ \theta_b]^T \in C^{base}_{space}$ and the configuration space of the continuum arm $c = [\omega\ u\ v] \in C_{space}$. Since motion planning for mobile robots

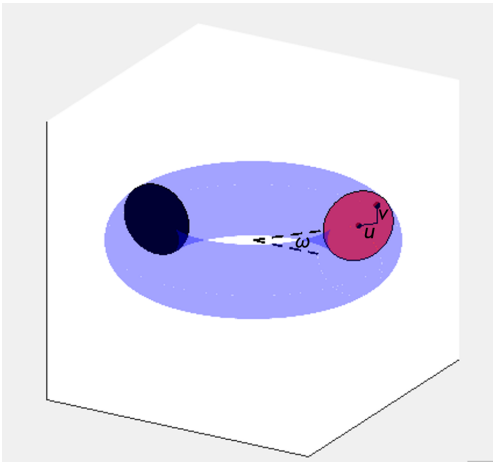

Fig. 10: C_{space} of CuRLE.

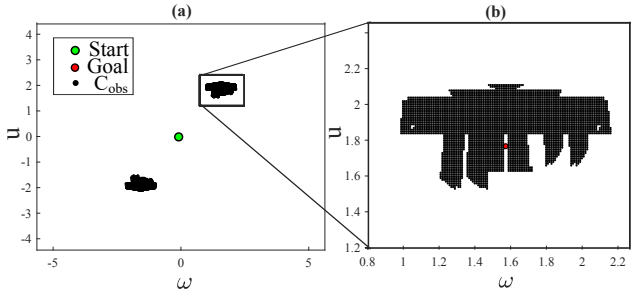

Fig. 11: The configuration space obstacles for the simulation scenario, along with the start configuration, are shown in (a), while (b) is the magnified obstacle from (a) where the goal configuration is located.

using their configuration space is well documented [6], we focus our efforts on the continuum arm.

B. Configuration Space of CuRLE

Recall that for a fixed arc-length s, a single section continuum robot has a practical configuration space of a circle bounded by $\theta = 2\pi$, shown in Fig. 3. Since the continuum arm of CuRLE can physically collide with the mobile base, we modify the boundary to $\theta \leq \pi\sqrt{2}$ (the value of the θ when $u = v = \pi$).

The revolute joint at the base of the continuum arm is described by $\omega \in [0, 2\pi)$. In the ideal case, ω displays the same "wrapping" behavior that the revolute joints in the rigid-link configuration space. As such, adding ω changes the configuration space to 3 dimensions by revolving the "uv-circle" around a central axis. The shape, depicted in Fig. 10, echoes the torus described by Q^2_{space}, the c-space of 2 revolute DoF. Unlike Q^2_{space}, however, CuRLE 's is "solid", i.e. true 3D, meaning that configurations c are not limited to the surface of the torus only. ω selects the "slice" (a circle) of the torus and u and v select the point c within that circle. Due to physical constraints, however, we limit $\omega \in [-\pi, \pi)$ and do not allow wrapping, which is represented in Fig. 10 by the solid black plane at $\omega = -\pi$.

C. Motion Planning with RRT and A*

Now that the configuration space for CuRLE has been established, we apply classical motion planning techniques to map and navigate the space.

A rapidly exploring random tree algorithm (RRT) was implemented using C++. Every node in the graph is a configuration $c \in C_{space}$ and every edge is the "action" vector δ needed to move from one configuration to the next. The start and goal location, along with the location of all configuration space obstacles, were known *a priori*. All of the obstacles are convex polyhedrons.

At every iteration of the RRT algorithm, a random configuration is generated and added to the closest node in the graph (barring no collisions). Every N iterations (starting with the first), the goal node is used instead of the random node. Collisions are detected by treating the continuum backbone as a series of finite spheres and sampling along the series while checking if the sampled sphere collides with any of the obstacles.

Given the unique kinematic constraints of continuum robots identified earlier, the RRT algorithm had to be modified to work for CuRLE . In order to pick up an object, a cup on a shelf for instance, the continuum arm has to bend in such a way so that the object ends between the fingers on the gripper. Since the gripper has a maximum width, the room for error is very small. In the configuration space, this means that the goal location is always in a narrow "canyon" created by the configuration space obstacles. For RRT implementations, this can make it very difficult to connect to the goal. We solved this issue by "projecting" the goal node along a straight line until it was out of the "canyon". Once this projected goal could be attached to the graph, the goal would then be achieved moving u or v in a straight line.

Once the RRT algorithm connected the goal configuration to the graph, we ran an A* algorithm to determine the optimal path (given the tree generated by the RRT). The A* used a heuristic of the L2-norm between a given configuration and the goal configuration. The cost function was the L2-norm between each node in the current path from the start node. The algorithm then output the full graph and optimal path.

As noted in our discussion of the configuration space for CuRLE, the mobile base and the continuum element can be considered independent, enabling the use of separate RRT algorithms for each space. We use the same core algorithm discussed above for each space. In our experimentation, we demonstrate the execution of the motion planning output in serial and in parallel.

D. Simulation

To verify the motion planning algorithms, a simulated environment was created in Matlab and a model of CuRLE was developed and added to the simulation. The simulation involves a scenario where CuRLE is instructed to pick up a cup off a shelf by the user. The task space obstacles were converted to configuration space obstacles, shown in Fig. 11. The start configuration of CuRLE $c_{start} = [0\ 0\ 0]^T$

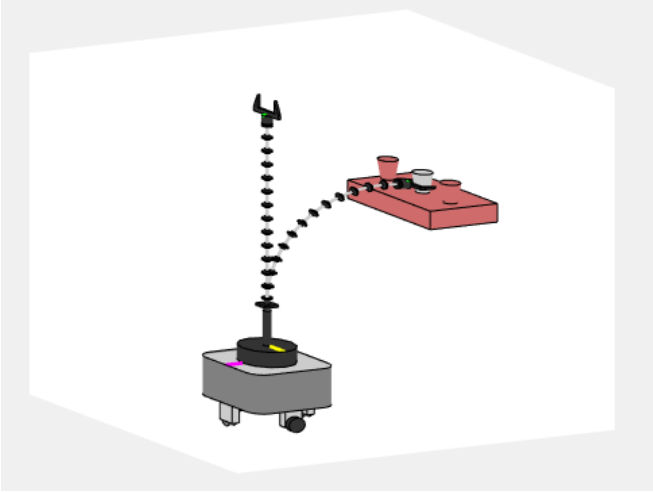

Fig. 12: The simulated CuRLE in the start (vertical) and goal (bent) configuration. The objective of the scenario was to pick up the light grey cup on the shelf.

and the goal configuration for the example reported herein was $c_{goal} = [\pi/2 \ \ 1.76 \ \ 0]^T$, (i.e. the configuration needed to pick up the cup). This goal was determined by using the interactive GUI developed with the environment to bend the simulated CuRLE until it was in the correct configuration.

The output of the RRT/A* was fed into the simulation and Fig. 12 shows CuRLE achieving the goal configuration of grasping the "cup". For this simulation, we set $v = 0$ to keep the configuration space 2D and allow for easy visualization of the nodes from the RRT algorithm.

E. Hardware Testing and Integration

After successfully running the simulation, we first tested the continuum controller's ability to "follow" an RRT path by serially executing the transition from node to node. We took the same RRT output (shown in Fig. 12) and passed this path to CuRLE. We issued "grasp" command to grab the cup and then passed CuRLE a second path from the RRT to lift the cup from the shelf. The results of this experiment are shown in Fig. 13.

To demonstrate the full functionality of the system, we explored a simple in-home scenario where the user has asked CuRLE to fetch a cup from shelf, bring the cup into an adjacent room and set it down on a different shelf, then navigate to its "docking station" in another portion of the smaller room. Images from the video footage recording these experiments are shown in Fig. 14, 15 and 16. For full details of the implementation, see [19].

V. CONCLUSIONS

We have analyzed the practical configuration space for a single section continuum robot and highlighted its unique features focusing on tendon actuated continuum sections. We have shown that classical motion planning techniques can be applied in much the same way as with standard robots, once certain features unique to continuum robots are taken into account.

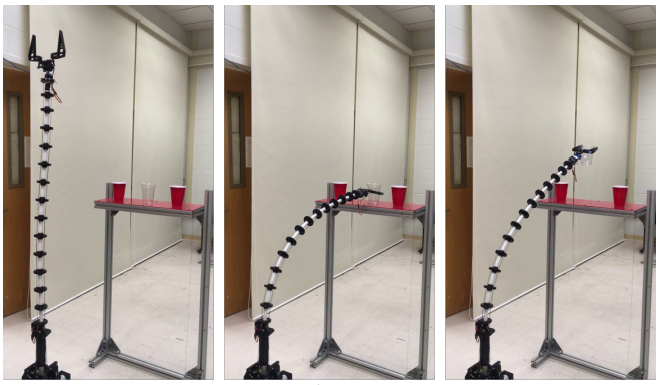

(a) (b) (c)

Fig. 13: (a) The state of CuRLE after ω has aligned with the goal ω. (b) CuRLE has grasped the cup. (c) The results of a second path generated by the RRT that guided CuRLE to pick the cup off the shelf.

The efforts presented here to define the configuration space for a single section, extensible continuum robot serves as a necessary stepping stone to the description and visualization of the c-spaces for multi-section extensible manipulators. In addition, this work expands the opportunity for the application of new motion planning methods that depend on the configuration space with respect to continuum robots.

REFERENCES

[1] D. Trivedi, C.D. Rahn, W.M. Kier, and I.D. Walker, "Soft Robotics: Biological Inspiration, State of the Art, and Future Research", Applied Bionics and Biomechanics, 5(2), pp. 99-117, 2008.

[2] R.J. Webster III and B.A. Jones, "Design and Kinematic Modeling of Constant Curvature Continuum Robots: A Review", International Journal of Robotics Research, Vol. 29, No. 13, pp. 1661-1683, November 2010.

[3] J. Burgner-Kars, D.C. Rucker, and H. Choset, "Continuum Robots for Medical Applications: A Survey", IEEE Transactions on Robotics, Vol. 31, No. 6, December 2015, pp. 1261-1280.

[4] I.D. Walker, H. Choset, and G. Chirikjian, "Snake-like and Continuum Robots", Chapter 20, in Springer Handbook of Robotics, Second Edition, pp. 481-498, 2016.

[5] J-C. Latombe, Robot Motion Planning, Kluwer, 1991.

[6] S.M. Lavalle, Planning Algorithms, Cambridge University Press, 2006.

[7] L.A. Lyons, R.J. Webster III, and R. Alterovitz, "Planning Active Cannula Configurations Through Tubular Anatomy", Proceedings IEEE International Conference on Robotics and Automation (ICRA), Anchorage, pp. 2082-2087, AK, 2010.

[8] A. Marchese, R.K. Katzschmann, and D. Rus, "Whole Arm Planning for a Soft and Highly Compliant 2D Robotic Manipulator", Proceedings IEEE/RSJ International Conference on Intelligent Robots and Systems (IROS), Chicago, IL, pp. 554-560, 2014.

[9] J. Xiao and R. Vatcha, "Real-Time Adaptive Motion Planning for a Continuum Manipulator", Proceedings IEEE/RSJ International Conference on Intelligent Robots and Systems (IROS), Taipei, pp. 5919-5926, 2010.

[10] J. Li, Z. Teng, J. Xiao, A. Kapadia, A. Bartow, and I.D. Walker, "Autonomous Continuum Grasping", Proc. IEEE/RSJ International Conference on Intelligent Robots and Systems (IROS), Tokyo, Japan, pp. 4569-4576, 2013.

[11] M. Neumann, and J. Burgner-Kahrs, "Considerations for Follow-The-Leader Motion of Extensible Tendon-driven Continuum Robots, Proceedings IEEE International Conference on Robotics and Automation (ICRA), Stockholm Sweden, May 2016, pp. 917-923.

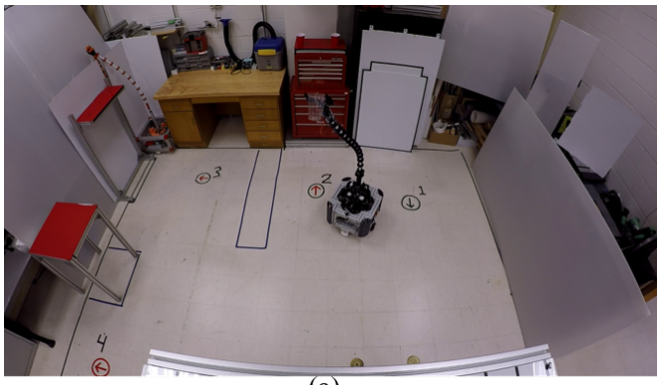

(a)

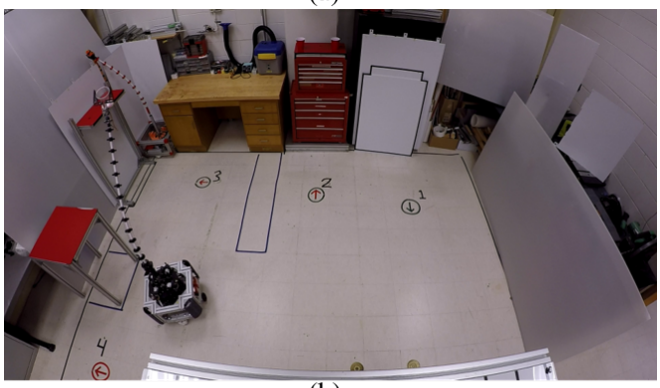

(b)

Fig. 14: (a-b) Results when CuRLE has been issued the command ”Go grab that cup off of the shelf”.

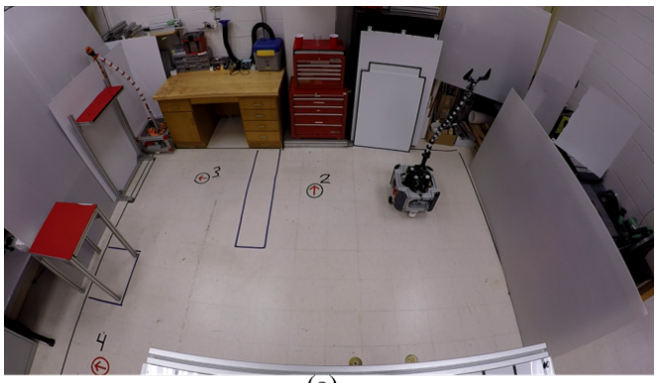

(a)

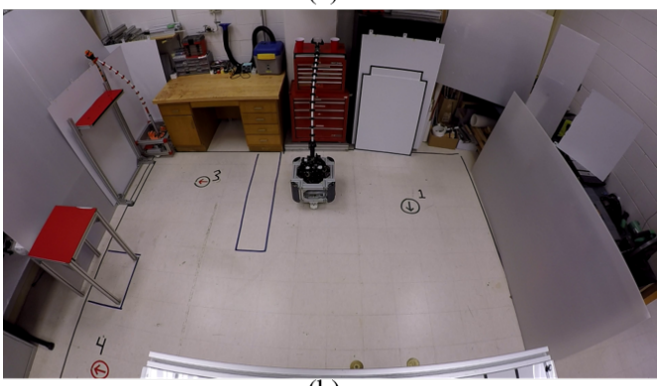

(b)

Fig. 15: (a-b) Results from when CuRLE has been issued the command ”Take the cup to the shelf in other room and set it down”.

[12] L.G. Torres and R. Alterovitz, “Motion Planning for Concentric Tube Robots Using Mechanics-based Models”, Proceedings IEEE/RSJ International Conference on Intelligent Robots and Systems (IROS), San Francisco, CA, pp. 5153-5159, 2011.

[13] L.G. Torres, C. Baykal, and R. Alterovitz, “Interactive-rate Motion Planning for Concentric Tube Robots”, Proceedings IEEE International Conference on Robotics and Automation (ICRA), Hong Kong, pp. 1914-, 2014.

[14] L.G. Torres, A. Kuntz, H.B. Gilbert, P.J. Swaney, R.J. Hendrick, R.J. Webster, III, and R. Alterovitz, “A Motion Planning Approach to Automatic Obstacle Avoidance During Concentric Tube Robot Teleoperation”, Proceedings IEEE International Conference on Robotics and Automation (ICRA), Seattle, WA, pp. 2361-2367, 2015.

[15] A. Kuntz, A.W. Mahoney, N.E. Peckman, P.L. Anderson, F. Maldonado, R.J. Webster, III, and R. Alterovitz, “Motion Planning for Continuum Incisionless Surgical Parallel Robots”, Proceedings IEEE/RSJ International Conference on Intelligent Robots and Systems (IROS), Vancouver, Canada, pp. 6463-6469, 2017.

[16] S. Verma, P. Gonthina, Z. Hawks, D. Nahar, Y. Wang, C. de Aguiar, J.O. Brooks, I.D. Walker, and K.E. Green,“Design and Evaluation of Two Robotic Furnishings Partnering with Each Other and Their Users to Enable Independent Living”, Proc.12th EAI International Conference on Pervasive Computing Technologies for Healthcare, ACM, New York City, NY, May 2018, pp. 35-44.

[17] W. Felt, M. T. and, T. Allen, G. Hein, J. Pompa, K. Albert, and D. Remy, “An inductance-based sensing system for bellows-driven continuum joints in soft robots,” in Robotics: Science and Systems, The Hague, Netherlands, 07 2017.

[18] Hannan, Michael W., and Ian D. Walker. ”Kinematics and the implementation of an elephant’s trunk manipulator and other continuum style robots.” Journal of robotic systems 20.2 (2003): 45-63.

[19] Z. Hawks, ”Motion Planning for a Continuum Robot Mobile Lamp”, Masters Thesis, Department of Electrical and Computer Engineering, Clemson University, 2019

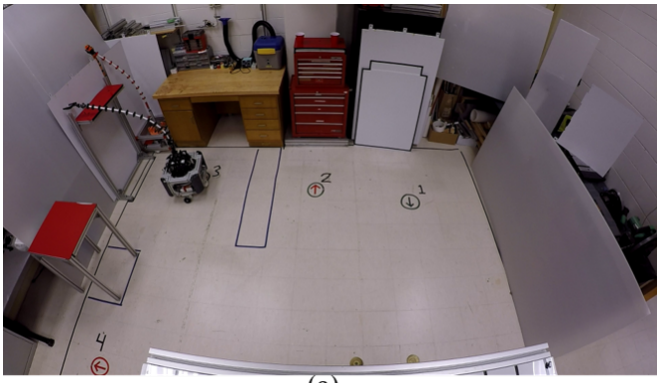

(a)

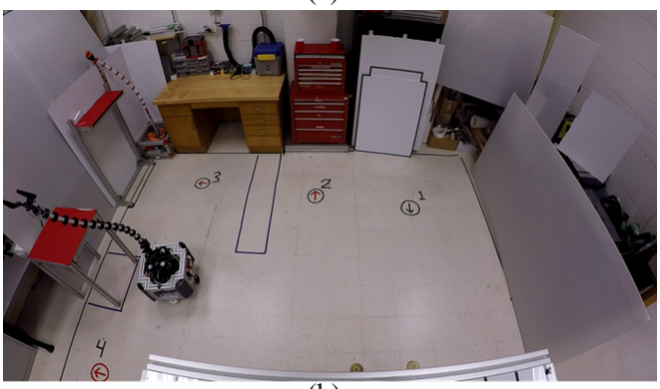

(b)

Fig. 16: (a) Results from when CuRLE has been issued the command ”Return to your docking station”.